Quantitative investigation of the formation of oxygenated aromatics in an anisole-doped flame

Kanika Sood, Sylvie Gosselin, Abderrahman El Bakali, Alessandro Faccinetto, Pascale Desgroux, Kevin van Geem, Laurent Gasnot, Luc-Sy Tran

Published in Proceedings of the Combustion Institute

https://doi.org/10.1016/j.proci.2024.105289

(accepted version)

Quantitative investigation of the formation of oxygenated aromatics in an anisole-doped flame

Kanika Sood[a], Sylvie Gosselin[a], Abderrahman El Bakali[a], Alessandro Faccinetto[a], Pascale Desgroux[a], Kevin M. Van Geem[b], Laurent Gasnot[a], Luc-Sy Tran[a,*]

[a]*Univ. Lille, CNRS, UMR 8522 - PC2A - Physicochimie des Processus de Combustion et de l'Atmosphère, F-59000 Lille, France.*

[b]*Laboratory for Chemical Technology (LCT), Ghent University, Technologiepark 125, B-9052 Ghent, Belgium*

Abstract

Recent studies have demonstrated that several oxygenated aromatics, including oxygenated polycyclic aromatic hydrocarbons (OPAHs) possessing different functional groups, are formed during anisole combustion. However, a quantitative analysis for these species is still very limited. This limitation inhibits the development and validation of formation kinetic mechanisms for these toxic air pollutants. This study addresses this gap by investigating quantitatively, a fuel-rich anisole-doped laminar premixed flame stabilized on a Holthuis burner at atmospheric pressure with an equivalence ratio of 1.90. Gas samples were extracted from the flame using a quartz nozzle and analyzed by gas chromatography (GC) preceded by a special online pre-concentration trap system, which decreases the detection limit by a factor of over 1000 compared to a conventional GC. Major species (reactants, CO, etc.), 32 small intermediates (C_1-C_5 like formaldehyde, acetaldehyde, acetylene, cyclopentadiene, etc.), 12 non-oxygenated aromatics (benzene, naphthalene, phenanthrene, etc.), and especially 24 oxygenated aromatics (phenol, 2,2-biphenol, dibenzofuran, 9H-xanthene...) including several OPAHs at ppb concentration levels were quantified. Interestingly, flame structure analysis shows that oxygenated aromatics peak closer to the burner surface as compared to non-oxygenated aromatics. The number of rings for non-oxygenated aromatics was observed to increase with the height above the burner, indicating that one-ring aromatics form before two- or three-ring aromatics. However, this is not always the case for oxygenated aromatics. Three-ring OPAHs are almost as abundant as the three-ring PAHs in terms of quantity, some three-ring OPAHs are even twice as abundant as their analogous PAHs (e.g., benzofuran vs fluorene, 9H-xanthene vs anthracene, etc.), which emphasizes their importance and certainly implies that these species need to be considered in kinetic studies. However, unlike PAHs, only less than half of the quantified OPAHs are currently present in literature models for anisole combustion.

Keywords: Lignin-based biofuel, anisole, flame, OPAHs, PAHs

---

*Corresponding author.

Dr. Luc-Sy Tran. Univ. Lille, CNRS, UMR 8522 - PC2A - Physicochimie des Processus de Combustion et de l'Atmosphère, F-59000 Lille, France. E-mail: luc-sy.tran@univ-lille.fr and luc-sy.tran@cnrs.fr.

Information for Colloquium Chairs and Cochairs, Editors, and Reviewers

1) Novelty and Significance Statement

The novelty of this study lies in the explicit quantification of OPAHs (and associated PAHs) in a fuel-rich laminar premixed anisole doped flame. Challenges associated with the experimental quantification of OPAHs from complex flame sample mixtures spanning a broad range of concentrations (several ppm to a few ppb) are overcome using different GC setups with online sample enrichment accessory. Comparison with non-oxygenated analogs presents pioneering observations like OPAHs are formed prior to PAHs in the studied conditions and that the abundance of a given species is related to the number of rings where the trend followed by OPAHs and PAHs is dissimilar. Our findings underscore the value of a sub-mechanism considering currently missing OPAHs in detailed kinetic mechanisms for anisole. The latter are necessary to achieve a safe integration of lignin-based biofuels in the auto-industry.

2) Author Contributions

- KS: Performed research, Analyzed data, Wrote and Reviewed the paper
- SG: Analyzed data, Reviewed the paper
- AEB: Analyzed data, Reviewed the paper
- AF: Analyzed data, Reviewed the paper
- PSD: Analyzed data, Reviewed the paper
- KMVG: Analyzed data, Reviewed the paper
- LG: Supervision, Analyzed data, Wrote and Reviewed the paper
- LST: Supervision, Performed research, Analyzed data, Wrote and Reviewed the paper

3) Authors' Preference and Justification for Mode of Presentation at the Symposium

The authors prefer **OPP** presentation at the Symposium, for the following reasons:

- A promising experimental database on the quantification of OPAHs necessary to improvise chemical kinetic mechanisms
- Acute challenges addressed in this work are of foremost importance for people performing speciation measurements in extremely complex flame samples
- The content of the paper constitutes intriguing results concerning emissions from lignin-based biofuel and a former comparison of OPAHs and PAHs
- In relevance to the theme of the 40th ISOC "emphasizing energy transition"

1. Introduction

Despite several unfavorable effects (CO_2 emissions, depletion of energy resources, etc.), global energy production from the combustion of fossil fuels continues to account for over 80% of the total energy produced across the world [1]. The use of renewable sources such as "bioenergy" including solid biomass and its liquid derived biofuels has been identified as one of sustainable solutions for mitigating global CO_2 emissions and improving energy security [2]. Lignin is one of the main components of biomass, taking about 10–30% of its weight [3], that has long been considered as a waste product in the pulp and paper industry, as well as in bioethanol production [4,5]. Several processes were recently proposed to convert lignin into a variety of valuable chemicals and fuels (i.e., "lignin-based biofuels") [6,7]. However, despite the potential presented by these biofuels, their combustion processes are likely to increase the formation of aromatic compounds, particularly oxygenated aromatics and OPAHs due to their chemical structure. OPAHs, recognized for their increased toxicity as compared to conventional aromatics [8,9], can significantly impact the characteristics of soot particles and exhaust gas emissions [10]. Recent research efforts have delved into the formation kinetics of OPAHs during combustion of fuels in general [11,12], with specific attention given to lignin-based biofuels [13,14]. Anisole or its derivatives were used in these studies as component models of lignin-based biofuels [13–16]. Anisole has suitable properties for internal combustion engines, e.g. high-octane number (RON=114) and high lower heating value (33 MJ/L *vs* 21.3 MJ/L for ethanol and 30.1-33.3 MJ/L for gasoline) [17]. Amongst recent studies, Chen et al. [13] and Sood et al. [18] demonstrated that a large number of oxygenated aromatics, including OPAHs, are formed during the oxidation of anisole. Despite recent progress in the identification of OPAHs during lignin-based biofuel combustion, quantitative analysis for these species is surprisingly still very limited, though quantitative data in laboratory-scale reactors is crucial to develop and validate kinetic models for these air pollutants. It is worth mentioning that the species quantified in the literature studies for anisole so far are rather limited to mainly benzofuran and dibenzofuran (see Section S1 in Supplemental Material 1, SM1), while recent studies on the identification of OPAHs show that their number can reach over 40 species [13,18].

Motivated by the potential of lignin biofuels, the potential issue of oxygenated aromatics formation, and the lack of quantitative analysis for these air pollutants, this study presents quantitative results from a fuel-rich anisole-doped flame.

Note that, under flame conditions, especially in premixed flames, PAHs are usually present in ppm levels [19] and it is expected that OPAHs would also be present in low or even lower concentrations which is why, experimentally, it is very challenging to quantify and study them. The experimental approach used in the present study has overcome this technical issue to explore a wide range of aromatics.

2. Experimental method

A laminar premixed stagnation flame burner coupled to 4 GC setups was used to carry out this work. A schematic representation is available in SM1 (Section S2).

2.1 Flame conditions

A fuel-rich premixed flame of anisole/iso-octane/methane was stabilized on a Holthuis burner at atmospheric pressure, with an equivalence ratio of 1.90, a total flow rate of 9.86 ln/min (normal liter per minute) and an overall mass flow rate per area of 7.82×10^{-3} g/cm^2/s. Fuel-rich conditions were chosen to facilitate the formation of aromatics. The fuel mixture contained 10% anisole and a liquid heavy hydrocarbon, inspired by the potential use of biofuels as additives in gasoline in real applications. Iso-octane was chosen as it is often used as a representative branched alkane and serves as a key component in gasoline surrogates [20]. Methane was needed to stabilize the flame. In this flame, 71.3% of the carbon originates from iso-octane and anisole, while 28.7% comes from methane. A flame without anisole was also measured under close fuel-rich conditions for comparison of product distribution. The detailed conditions of these flames are provided in Section S2. The burner system was detailed previously [18,21]. Briefly, the burner central porous (60 mm in diameter, with cooling water kept at 60°C) was surrounded by another co-annular porous used for the nitrogen shroud (25 ln/min) to protect the flame from perturbations by the surrounding air. To stabilize the fuel-rich flame, a stagnation plate (stainless-steel disc with 60 mm diameter and 30 mm thick) was surmounted at 21 mm above the burner surface and was pierced at its center to provide access for a quartz nozzle.

The liquid flow rates of anisole and iso-octane (Sigma-Aldrich, purity 99.0%) were controlled by a dual-liquid vaporization system. This system constituted two Coriolis flow controllers (Bronkhorst, error ±0.2%) followed by two evaporators/mixers, in which liquid fuels were vaporized and mixed with N_2. The gaseous stream was then mixed with O_2 and CH_4 and fed to the burner. Flow rates of CH_4, O_2 and N_2 (Air Liquide, purity >99.95%) were controlled using Mass Flow Controller (MFC, Bronkhorst, error ±0.5%).

The flame temperature as a function of the height above the burner (HAB) was measured using thermocouple-based thermometry with soot deposition correction and radiation loss correction based on extrapolation to zero wire diameter, as employed in [22]. The temperature measurement

approach was chosen also in comparison with additionally performed laser-induced fluorescence measurements. More details concerning this method are provided in SM1 (Section S3).

2.2. Species measurements by GCs

Gas samples were extracted from the flame using a quartz nozzle (190 µm orifice, 0.9 mm tip, 24° opening angle) and directed to the GCs via a heated sampling line (~140° C). Four GCs were used to analyze the sample.

The first GC (GC Perkin Elmer Clarus 580), which was detailed previously [23], comprises of a capillary column Rt-Q Bond (30 m × 0.25 mm × 8 µm, 100% divinylbenzene, Restek), a TCD and a FID preceded by a methanizer (nickel catalyst for hydrogenation). This system enabled the quantification of major species (fuels, CO, CO_2, H_2), small hydrocarbons, small oxygenated species and some monoaromatics (benzene, cresols, etc.). Calibration factors were determined using cold-gas mixtures whenever available or by relying on the hydrogenation using the methanizer to convert species to their corresponding alkane. This procedure was proven successful previously [23]. The estimated uncertainties of data from this GC are nearly <15% for main species, <25% for abundant intermediates, and <55% for minor products (<10 ppm). The estimation was based on the error of the MFCs used, the error of the composition of commercially available standard mixtures, the calibration method, and the signal-to-noise ratio.

A second GC (GC-Scion 456) equipped with an FID and an online Sample Pre-concentration Trap (SPT) system (called here "GC-SPT-FID") was used for quantifying mainly PAHs and OPAHs. As PAHs and OPAHs are usually present in concentrations that are too low to be correctly determined by a regular GC, the SPT, a sample enrichment device, was used. This pre-concentrating system operates on the idea of cryofocusing–thermodesorption which is a common and powerful technique to perform quantification of species at trace levels. The gaseous flame sample was preconcentrated on inert adsorptive glass beads at a specific adsorption temperature (-50°C) using a coolant (liquid N_2). Through subsequent rapid heating of the adsorptive material to a desorption temperature (200°C), the steady state was instantaneously shifted towards desorption (thermodesorption), consequently remobilizing the trapped analytes. Formerly trapped analytes were then flushed in the opposite direction to the sampling flow, onto the chromatographic column dedicated for aromatics (SCION-17MS; 30 m × 0.32 mm × 0.25 µm, 50% phenyl methylpolysiloxane as stationary phase) and detected with an FID. An illustration of the different steps involved in SPT is provided in SM1 (Section S2).

Aromatics were identified by their mass spectra and their individual retention times from pure product injection when available. Because of the highly complex aromatic composition of flame samples, two GC-MS setups with two separation mechanisms, a 1D GC-MS (Agilent Technologies 5975C) and a 2D GC-MS (GC×GC, Thermo Scientific Trace GC Ultra), with electron ionization at 70 eV, were used for identification. The identification methodology was detailed in our previous work [18]. More technical details of these setups are available in SM1 (Section S2).

3. Results and discussions

Section 3.1 briefly presents the temperature, fuels and major end products, and Section 3.2 presents selected C_1-C_5 intermediates, followed by discussions on mono-aromatics, PAHs and OPAHs in Section 3.3. While a full list of the quantified species is available in SM1 (Section S5) and the data is available in SM2, important examples are presented and discussed in the following sections. Carbon balance was checked and it is close to 100% (e.g. 102 % at HAB=2.55 mm).

3.1. Temperature, fuels and major end products

Fig. 1 presents the flame temperature profiles measured with and without the sampling nozzle as well as the mole fraction profiles of the fuels, O_2, H_2, CO, and CO_2. The lowest temperatures measured are about ~1000-1200 K close to the surface of the burner, whereas the maximum temperatures range around 1700-1750 K at HAB ~ 3-4 mm) and decrease to about 1500-1600 K towards the stabilization plate. The presence of the nozzle shifts the temperature profiles ~1 mm towards the burnt gas zone. Anisole and iso-octane are no longer detectable from about 3 mm, and O_2 from about 5 mm. The used equivalence ratio is far from the stoichiometric conditions leading to incomplete oxidation process that explains the high mole fractions of CO (0.164 vs. 0.045 for CO_2).

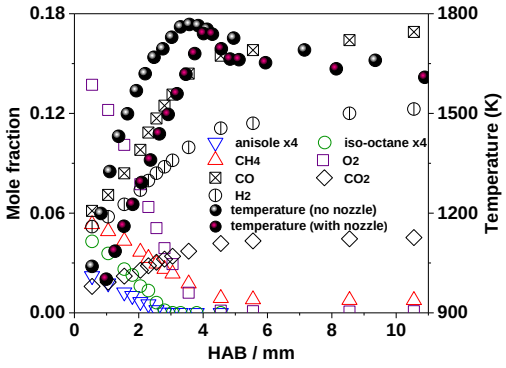

Fig. 1. Temperature, reactant, and major end products.

3.2. C_1-C_5 intermediate species

Fig. 2 presents the mole fraction profiles of selected species amongst >30 C_1-C_5 intermediate species, such as formaldehyde, acetylene, propene,

iso-butene, and cyclopentadiene. Formaldehyde peaks at HAB ~ 2 mm, while others peak at about 2.5-3.0 mm. These species have peak mole fraction of 7.96×10^{-4}, 1.39×10^{-2}, 1.73×10^{-3}, 2.18×10^{-3}, and 3.70×10^{-4}, respectively, and are the most abundant intermediate within their carbon number group, respectively. Formaldehyde is highly toxic and reactions of C_2-C_5 unsaturated hydrocarbons can contribute to the formation of the first aromatic ring. The mole fraction of acetylene largely predominates under these flame conditions making it the most abundant not only amongst C_2 species but also amongst all intermediates. This species persists with high amounts in the burnt gas zone, and is well-known to participate to the PAH growth via the HACA mechanism (H-abstraction-C_2H_2-addition) [24].

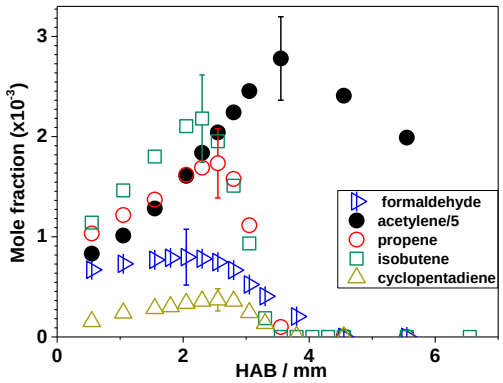

Fig. 2. The most abundant C_1-C_5 intermediates. Error bars are included

3.3. Aromatic species

A total of 36 aromatics including 12 non-oxygenated and 24 oxygenated are quantified. These numbers are quite noteworthy and a significant improvement over the available literature studies on absolute quantification. Benzene (C_6H_6, *m*/*z* 78) and phenol (C_6H_6O, *m*/*z* 94) are the smallest quantified non-oxygenated and oxygenated aromatics, respectively. The heaviest PAHs and OPAHs quantified in the present work are anthracene ($C_{14}H_{10}$, *m*/*z* 178) and diphenoxy methane ($C_{13}H_{12}O_2$, *m*/*z* 200). A typical chromatogram obtained by GC-SPT-FID for aromatics is shown in Fig. 3. The co-existence of PAHs and OPAHs in the studied flame is evident. Given the complexity inherent in this co-existence, the present experiments are limited to 3-ring aromatic species, and the heavier aromatics are a subject of perspective studies. The chromatogram in Fig. 3 is obtained at a low HAB where the concentration of PAHs is still low while higher levels of OPAHs are detected. Even after exhaustive identification, about 13 signals remain unidentified.

Since most of the PAHs and OPAHs are solid at room temperature, a special calibration procedure for GC-SPT-FID was used. In this method, the species of interest (PAH or OPAH) is stored in a cell for which the temperature and pressure are regulated. The concentration of the PAH or OPAH vapors generated by this system is calculated based on their saturation vapor pressure. The outlet of this cell is connected to the flame sampling line to transfer the generated samples to the GC. A schematic representation and more details are available in SM1 (Section S4). Besides other common uncertainty sources from GC, flame and sampling systems, the uncertainty of the PAH/OPAH calibration system also needs to be considered, for instance, the uncertainty of the vapor pressure data (for example ±5% for dibenzofuran [25]), two N_2 MFCs (±0.5% × 2 = ±1%), pressure sensor (±0.25%), and thermocouple for temperature (±1%). Also considering the error from the MFCs used for flame (±0.5% × 6 = ±3%), that from the influence of the noise of baseline on PAH/OPAH peak integration (±5-15%, depending on species' abundance), and the repeatability (<5%), the overall uncertainty of these molecules measured by GC-SPT-FID is estimated to be within ~20% (from ppm level) and ~30% (close to ppb level), except phenolics.

Prior to discussing each aromatic species, an overview on the position of peak mole fraction and the sum of maximum mole fractions of 1-, 2-, 3-ring aromatics is presented in Fig. 4. It is interesting to note that, in general, oxygenated aromatics attain their peak mole fractions before those of non-oxygenated aromatics. As shown in the left panel, the profiles of oxygenated aromatics are comparatively closer to the burner with respect to the non-oxygenated aromatics which suggests that these species could be produced before the non-oxygenated ones. Also, it is interesting to note that the number of rings for non-oxygenated species increase with HAB, indicating that one-ring species are formed prior to two- and three-ring species. However, this is not the case for oxygenated aromatics. Three-ring OPAHs appear to form as soon as one-ring oxygenates are formed (more details below). The bar graph on the right represents the sum of the peak mole fractions of all species (non-oxygenated and oxygenated) with the same number of rings. A comparison of the sum of the peak mole fractions of 1-, 2-, and 3-ring aromatics suggests that non-oxygenated aromatics are produced in higher amounts than oxygenated aromatics as far as one- and 2-ring aromatics are concerned. However, it can be seen that the sum of the amounts of 3-ring OPAHs are almost as abundant as the sum of the amounts of the 3-ring PAHs.

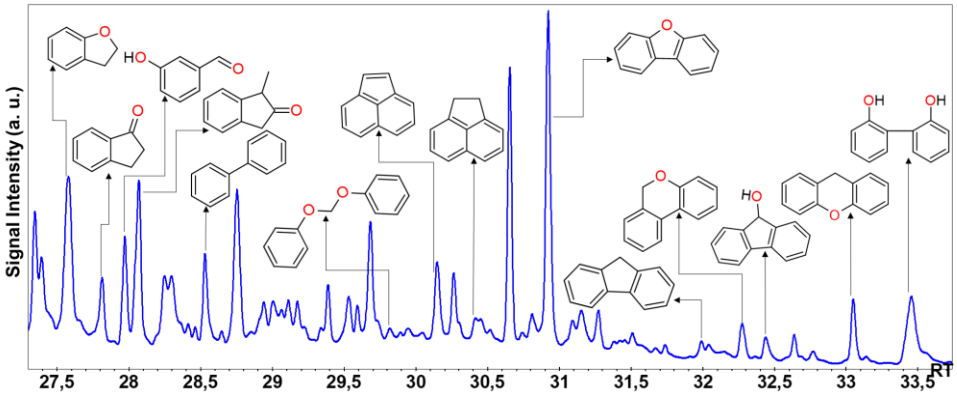

Fig. 3. Typical chromatogram (zoom between 27-34 min) obtained by GC-SPT-FID for the anisole doped flame at 2 mm.

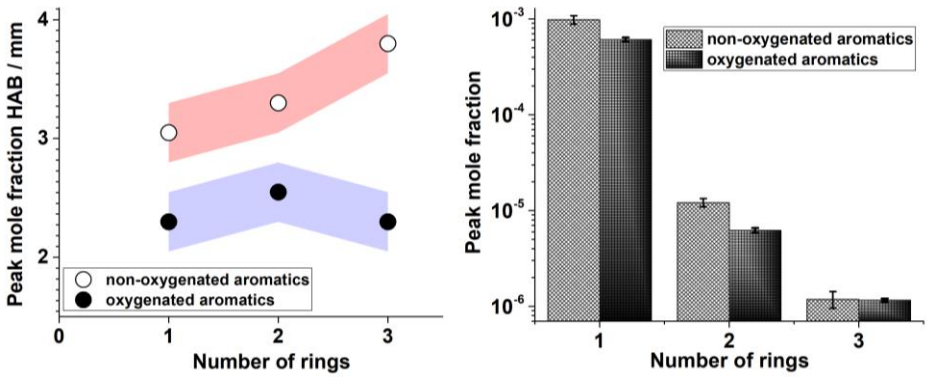

Fig. 4. Overview on the position of peak mole fraction profiles and comparison of the sum of maximum mole fractions of 1-, 2-, 3-ring aromatics. Error areas (left) or error bars (right) are included.

Fig. 5 presents a detailed analysis of all the aromatics quantified in this study. Panel (a) presents a bar graph representation of the peak mole fractions of all the quantified aromatics. As shown in the figure, oxygenated aromatics and OPAHs constitute a significant fraction of anisole decomposition products under the studied conditions. Anisole can readily undergo the O-CH_3 bond dissociation because of its very low bond dissociation energy to form the phenoxy radical, whose implication in the combustion chemistry of anisole gives rise to a whole new set of stable intermediates such as simple and/or substituted phenol, cresols, benzofurans, indanones, xanthenes, xanthones and dioxin like species. The majority of 2- and 3-ring OPAHs are being quantified for the first time. The species are listed in the order of their respective amounts where phenol is the most abundant oxygenated aromatic whose concentration can range in hundreds of ppm whereas 2-dibenzofuranol is the least abundant quantified OPAH present in ppb levels. Panel (b) presents a comparison of the evolution of the mole fraction profiles of selected oxygenated aromatics together with their non-oxygenated analogs. Note that only experimental results are discussed here, simulations from the model of Ref [26] are also included for comparison but are discussed in the next paragraph. As stated earlier, oxygenated aromatics are found to peak earlier than their non-oxygenated analogs. This is true for all oxygenated aromatics irrespective of the number of rings present in their structure. For 1-ring species, benzene is more abundant than phenol. But it can be seen it is not certainly the case for 2- and 3-ring species. Benzofuran is slightly more abundant than indene whereas other species like dibenzofuran, xanthene and 6H-dibenzo [b,d] pyran are present in much higher amounts (more than twice) as compared to their non-oxygenated analogs i.e., fluorene, anthracene and phenanthrene respectively. Species like dibenzofuran, xanthene and 6H-dibenzo [b,d] pyran attain their peak mole fractions at similar HAB as that for phenol. This hints at earlier formation of 3-ring OPAHs in comparison to their analogous PAHs which are anticipated to be formed via the classical HACA mechanism [24] and are consequently formed much later. Mole fraction profiles of selected

aromatics from the same figure are also available collectively in SM (Fig. S7).

While the focus of this work is on experimental analysis, it is interesting to identify what quantified aromatics are present in the anisole-iso-octane models in the literature. There are numerous models developed for the pyrolysis/oxidation of anisole or iso-octane [14,15,26–31]. Surprisingly only two models contain the reaction mechanisms of anisole and iso-octane simultaneously [26,28], and only one amongst these two models contains 3-ring PAHs and OPAHs (i.e., the "CRECK model" [26]). As highlighted in Fig. 5a (bold structures), all non-oxygenated aromatics detected in the present flame were also found in the mentioned models, in particularly the CRECK model. However, 6 out of 24 quantified oxygenated aromatics were considered in the models. Dibenzofuran is the sole 3-ring OPAH considered in (some of) these models. Simulations using the CRECK model and the "Premixed Laminar Burner-Stabilized Stagnation Flame" module of Chemkin Pro [32], along with the measured temperature profile without any offset, are compared with experimental results for major species, abundant intermediates (Section S6 in SM1), and selected aromatics (Fig. 5b). Fig. 5b indicates that the model in general reproduces non-oxygenated aromatics well but significantly overpredicts oxygenated aromatics, with phenol, benzofuran, and dibenzofuran being overestimated by factors of 5, 40, and 30, respectively. However, the model accurately captures some relative trends, such as OPAHs like benzofuran and dibenzofuran peaking at lower HABs compared to their PAH counterparts, indene and fluorene respectively. Additionally, benzofuran and dibenzofuran are predicted to have higher mole fractions than indene and fluorene, which is consistent with experimental observations. It should be noted that detailed comparisons and discussions of model-experiment discrepancies are beyond the scope of this study; the modeling is primarily used to confirm and explain certain experimentally observed trends for PAHs and OPAHs.

Based on kinetics proposed in the CRECK model [26], some possible formation pathways for some relevant quantified species are presented in Fig. 6. The figure shows that 3-ring PAHs (e.g., phenanthrene and fluorene) are formed through 1- and 2-ring species, explaining the increase in HAB with the number of rings, as seen in Fig. 4. However, the formation of oxygenated aromatics does not always follow this mechanism (Fig. 6). Simulated profiles of some aromatics in Fig. S10 confirm this trend. Fig. 6 illustrates that phenol forms first and then leads to benzene. This pattern is also observed for o-cresol and toluene. Moreover, benzofuran and dibenzofuran are rapidly produced through the combination of phenoxy radicals, which are key early-stage fuel radicals. In simple terms, oxygenated aromatics are early products of anisole combustion, while non-oxygenated aromatics are secondary products and are produced through a multistep PAH growth process. Furthermore, the oxidation of OPAHs (e.g. dibenzofuran) also contributes to the formation of PAHs (e.g. naphthalene) (Fig. 6). The above-mentioned mechanisms could explain why oxygenated aromatics peak earlier than their non-oxygenated counterparts and are formed in high amounts. It is important to note that while this explanation is mainly based on formation kinetics, other factors such as molecular stabilization may also play a role. Isolating these factors for a more detailed study is challenging and will require another further investigation.

Based on the present experimental indications, as a first initiation, possible formation pathways of some selected newly-detected OPAHs are presented in Fig. 6 (bottom panel). The combination of phenoxy radical with the benzyl radical or its self-recombination can lead to the formation of 9H-xanthene or dibenzo-p-dioxin, respectively. Again, it can explain why they are produced earlier and in greater concentration compared to their analogous PAHs. While the formation of dibenzo-p-dioxin via this pathway was investigated in the literature [33], the formation of xanthene via this way is suggested by the detection of o-benzylphenol in the present work. The detection of diphenoxy methane and benzyl phenyl ether could be envisaged from the recombination of anisyl radical with the phenoxy and phenyl radicals, respectively, which suggests that not only phenoxy but also anisyl are important in the formation of OPAHs and need to be considered in the future models. The OPAH formation pathways discussed here are primarily focused on anisole as their precursor. However, it is worth noting that OPAHs could also form from PAHs, although this contribution might be deemed less substantial compared to the direct pathways involving anisole. This inference is supported by the absence of any OPAHs observed in another flame lacking anisole that was also studied (flame conditions showed in SM1). For comparison, this flame without anisole was also analyzed, which showed that while all non-oxygenated aromatics depicted in Fig. 5a were produced, they appeared in much lower quantities, and no oxygenated aromatics were detected in measurable amounts. Nonetheless, the potential interactions between species pools from iso-octane

and anisole reactions in the anisole-doped flame, which could affect the measured PAHs and OPAHs, cannot be ruled out. A recent study indicated that radicals from iso-octane might contribute to the formation of specific mono-ring oxygenated aromatics, such as 4-(2-methylprop-2-en-1-yl) phenol and [(2-methylprop-2-en-1-yl)oxy]benzene [18]. However, these species could not be quantified in the present work due to peak integration issues, preventing further discussion on the potential interactions. This is an interesting point that warrants further investigation in the future.

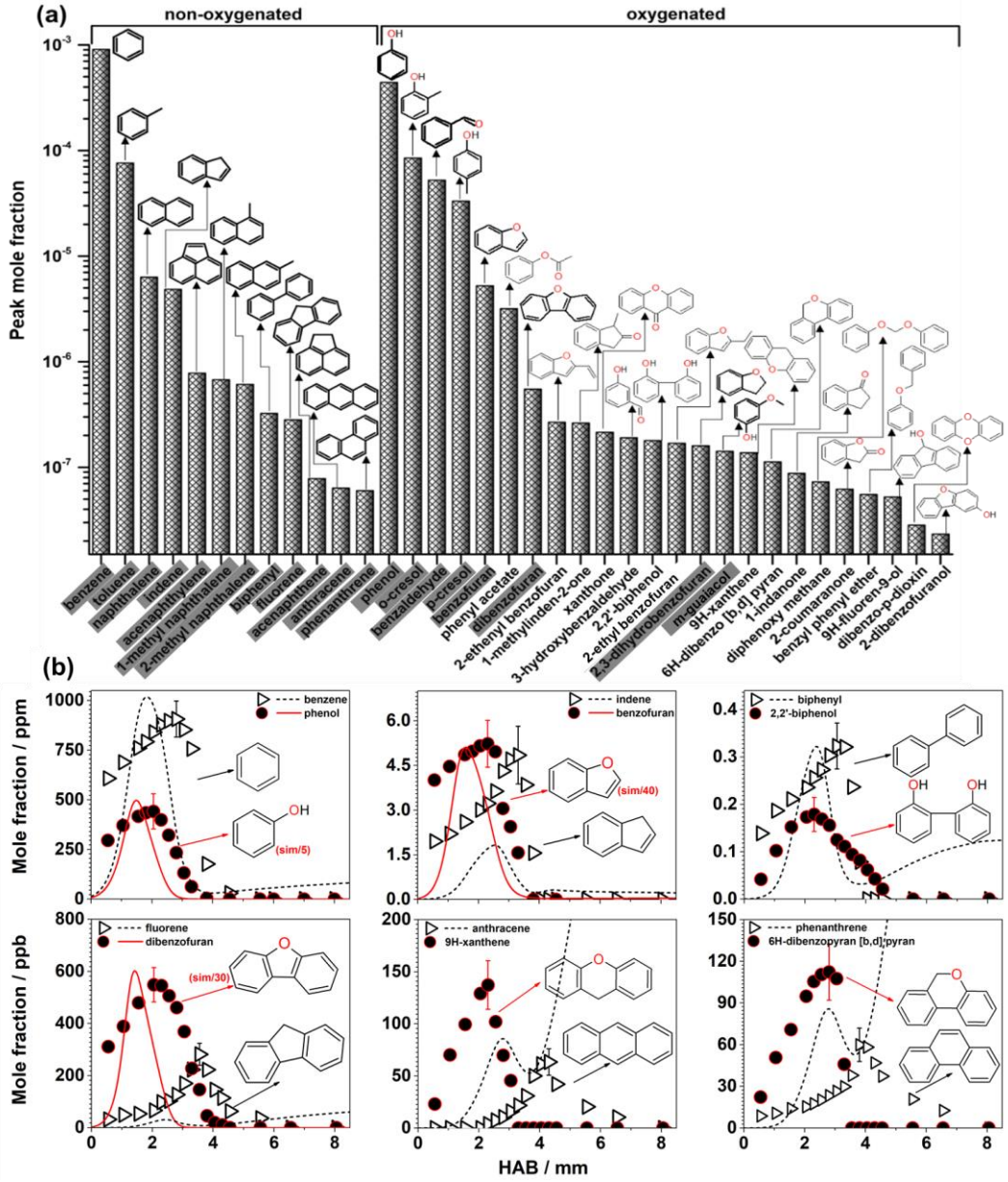

Fig. 5. Details of quantified aromatics. (a) A bar graph representation of the experimental results where shaded names on the x-axis are already considered in the literature models. (b) Selected mole fraction profiles of analogous structures where symbols represent data points determined experimentally and lines represent simulations from the CRECK model; for clarity, a division factor "f" was applied for some simulated profiles (shown as "sim/f"); simulated profiles of anthracene and phenanthrene, originally lumped together in the model, are divided by a factor of two to be considered for comparison with the experimental data points.

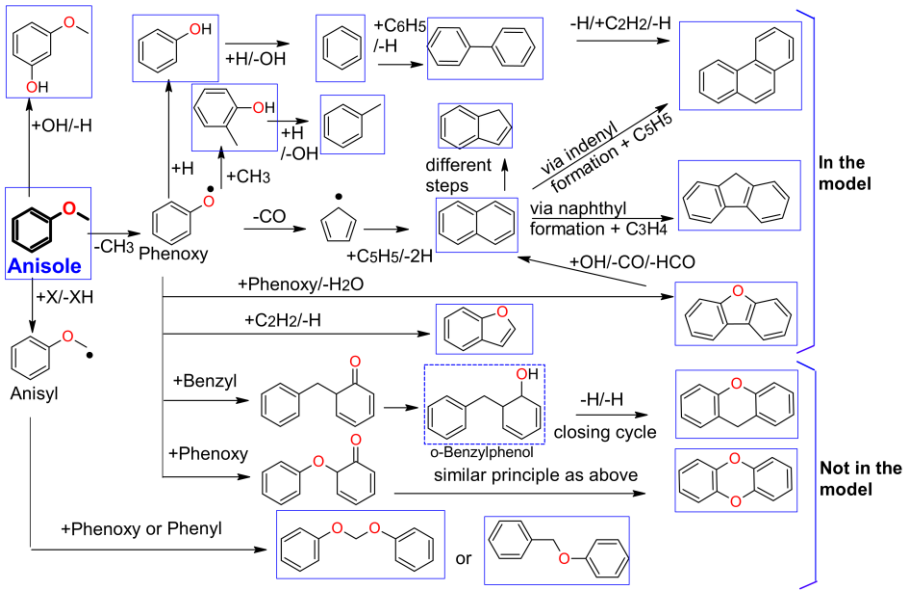

Fig. 6. Possible formation routes for selected aromatics, determined either based on the CRECK model [26] or proposed based on the current experimental evidence from this study. Species highlighted using solid boxes were experimentally quantified (species names are available in Fig. 5), whereas those using a dashed box were only identified.

4. Conclusions and perspectives

This study lays emphasis on the consequential co-existence of oxygenated and non-oxygenated aromatics in an anisole flame and reveals its tendency to form a variety of OPAHs which are challenging species to study. A sample enrichment device i.e., the 'SPT' system is adopted for quantification of species. The present study is so far the first quantitative study to highlight the implication of oxygenated aromatics and OPAHs in anisole-iso-octane doped laminar premixed flames where these species are not only experimentally quantified but also compared to their non-oxygenated analogs. In general, oxygenated aromatics are formed very close to the burner surface and their abundance decreases as the number of rings in a given structure increase. In comparison with non-oxygenated analogs, it was observed that though 1- and 2-ring non-oxygenated species are more abundant than 1- and 2-ring oxygenated aromatics, the inverse is true for 3-ring aromatics. Future research could explore the impact of varying amounts of anisole, address specific uncertainties in the calibration of phenolics, and focus on advancements in kinetic modeling.

Declaration of competing interest

The authors declare that they have no known competing financial interests or personal relationships that could have appeared to influence the work reported in this paper.

Acknowledgements

The authors would like to thank the financial support from ADEME, Hauts-de-France Region, IREPSE, and I-SITE (project "Biofuel-Soot" R-JEUNES CHERCHEURS-19-010-TRAN). The work was further supported by the Labex CaPPA and the CPER research project ECRIN. The authors express gratitude to Romain Laboure for his assistance with pure OPAH analyses, and to Dr. Shunsuke Suzuki for his valuable discussions regarding kinetic models.

Supplementary material

Two supplemental materials. 1/ PDF file: Additional information for experimental setup and results. 2/ Excel file: Experimental data

References

[1] IEA (2022), World Energy Outlook 2022, IEA, Paris https://www.iea.org/reports/world-energy-outlook-2022, License: CC BY 4.0 (report); CC BY NC SA 4.0 (Annex A).

[2] H.K. Jeswani, A. Chilvers, A. Azapagic, Environmental sustainability of biofuels: a review, Proc. R. Soc. Math. Phys. Eng. Sci. 476 (2020) 20200351.

[3] X. Lu, X. Gu, A review on lignin pyrolysis: pyrolytic behavior, mechanism, and relevant upgrading for improving process efficiency, Biotechnol. Biofuels Bioprod. 15 (2022) 106.

[4] F. Cotana, G. Cavalaglio, A. Nicolini, M. Gelosia, V. Coccia, A. Petrozzi, L. Brinchi, Lignin as co-product of second generation bioethanol production from ligno-cellulosic biomass, Energy Procedia 45 (2014) 52–60.

[5] S. Suresh, V. Viswanathan, M. Angamuthu, G.P. Dhakshinamoorthy, K.P. Gopinath, A. Bhatnagar, Lignin waste processing into solid, liquid, and gaseous fuels: a comprehensive review, Biomass Convers. Biorefinery 13 (2023) 4515–4553.
[6] J. Ma, S. Shi, X. Jia, F. Xia, H. Ma, J. Gao, J. Xu, Advances in catalytic conversion of lignocellulose to chemicals and liquid fuels, J. Energy Chem. 36 (2019) 74–86.
[7] D. Chiaramonti, M. Buffi, P. Palmisano, S. Redaelli, Lignin-based advanced biofuels: a novel route towards aviation fuels, Chem. Eng. Trans. 50 (2016) 109–114.
[8] S. Lundstedt, P.A. White, C.L. Lemieux, K.D. Lynes, I.B. Lambert, L. Öberg, P. Haglund, M. Tysklind, Sources, fate, and toxic hazards of oxygenated polycyclic aromatic hydrocarbons (PAHs) at PAH-contaminated sites, AMBIO J. Hum. Environ. 36 (2007) 475–485.
[9] M. Kawano, S. Uno, J. Koyama, E. Kokushi, A. McElroy, Effects of oxygenated polycyclic aromatic hydrocarbons on the early life stages of Japanese medaka, Environ. Sci. Pollut. Res. 24 (2017) 27670–27677.
[10] L. Xu, Y. Wang, D. Liu, Effects of oxygenated biofuel additives on soot formation: A comprehensive review of laboratory-scale studies, Fuel 313 (2022) 122635.
[11] X. Shi, Q. Wang, A. Violi, Chemical pathways for the formation of benzofuran and dibenzofuran in combustion, Combust. Flame 212 (2020) 216–233.
[12] P. Liu, B. Chen, Z. Li, A. Bennett, S. Sioud, S.M. Sarathy, W.L. Roberts, Evolution of oxygenated polycyclic aromatic hydrocarbon chemistry at flame temperatures, Combust. Flame 209 (2019) 441–451.
[13] B. Chen, S. Kruse, R. Schmid, L. Cai, N. Hansen, H. Pitsch, Oxygenated pah formation chemistry investigation in anisole jet stirred reactor oxidation by a thermodynamic approach, Energy Fuels 35 (2021) 1535–1545.
[14] B. Chen, M. Hellmuth, S. Faller, L. May, P. Liu, L. Cai, W.L. Roberts, H. Pitsch, Exploring the combustion chemistry of anisole in laminar counterflow diffusion-flames under oxy-fuel conditions, Combust. Flame 243 (2022) 111929.
[15] W. Yuan, T. Li, Y. Li, M. Zeng, Y. Zhang, J. Zou, C. Cao, W. Li, J. Yang, F. Qi, Experimental and kinetic modeling investigation on anisole pyrolysis: Implications on phenoxy and cyclopentadienyl chemistry, Combust. Flame 201 (2019) 187–199.
[16] M. Nowakowska, O. Herbinet, A. Dufour, P.A. Glaude, Kinetic study of the pyrolysis and oxidation of guaiacol, J. Phys. Chem. A 122 (2018) 7894–7909.
[17] F. Battin-Leclerc, N. Delort, I. Meziane, O. Herbinet, Y. Sang, Y. Li, Possible use as biofuels of monoaromatic oxygenates produced by lignin catalytic conversion: A review, Catal. Today 408 (2023) 150–167.
[18] K. Sood, S. Gosselin, M. Seifali Abbas-Abadi, N. De Coensel, J.-C. Lizardo-Huerta, A. El Bakali, K.M. Van Geem, L. Gasnot, L.-S. Tran, Experimental detection of oxygenated aromatics in an anisole-blended flame, Energy Fuels 38 (2024) 6355–6369.
[19] T. Bierkandt, P. Hemberger, P. Oßwald, D. Krüger, M. Köhler, T. Kasper, Flame structure of laminar premixed anisole flames investigated by photoionization mass spectrometry and photoelectron spectroscopy, Proc. Combust. Inst. 37 (2019) 1579–1587.
[20] R. Kumar, S. Kumar, Formulation of a three-component gasoline surrogate model using laminar burning velocity data at elevated mixture temperatures, Fuel 306 (2021) 121581.
[21] K. Sood, S. Gosselin, J.C.L. Huerta, A.E. Bakali, M.S. Abbas-Abadi, N. De Coensel, K.M. Van Geem, L.-S. Tran, Detection of oxygenated aromatics in atmospheric anisole flames, Proceeding 11th Eur. Combust. Meet. April 26-28 2023 Rouen Fr. (2023).
[22] J. Elias, A. Faccinetto, S. Batut, O. Carrivain, M. Sirignano, A. D'Anna, X. Mercier, Thermocouple-based thermometry for laminar sooting flames: Implementation of a fast and simple methodology, Int. J. Therm. Sci. 184 (2023) 107973.
[23] L.-S. Tran, H.-H. Carstensen, N. Lamoureux, K.K. Foo, S. Gosselin, A. El Bakali, L. Gasnot, P. Desgroux, Exploring the flame chemistry of C5 tetrahydrofuranic biofuels: tetrahydrofurfuryl alcohol and 2-methyltetrahydrofuran, Energy Fuels 35 (2021) 18699–18715.
[24] H. Wang, M. Frenklach, Calculations of rate coefficients for the chemically activated reactions of acetylene with vinylic and aromatic radicals, J. Phys. Chem. 98 (1994) 11465–11489.
[25] X.-W. Li, E. Shibata, E. Kasai, T. Nakamura, Vapour pressure determination for dibenzo-p-dioxin, dibenzofuran, octachlorodibenzo-p-dioxin and octachlorodibenzofuran using a Knudsen effusion method, Mater. Trans. 43 (2002) 2903–2907.
[26] CRECK modeling group: Anisole model. "CRECK_2003_TOT_HT_SOOT" Version. https://creckmodeling.chem.polimi.it/menu-kinetics/menu-kinetics-detailed-mechanisms/ (accessed April 11, 2024).
[27] S. Roy, O. Askari, Detailed kinetics for anisole oxidation under various range of operating conditions, Fuel 325 (2022) 124907.
[28] C.S. Mergulhão, H.-H. Carstensen, H. Song, S.W. Wagnon, W.J. Pitz, G. Vanhove, Probing the antiknock effect of anisole through an ignition, speciation and modeling study of its blends with isooctane, Proc. Combust. Inst. 38 (2021) 739–748.
[29] R.D. Büttgen, M. Tian, Y. Fenard, H. Minwegen, M.D. Boot, K.A. Heufer, An experimental, theoretical and kinetic modelling study on the reactivity of a lignin model compound anisole under engine-relevant conditions, Fuel 269 (2020) 117190.
[30] S.W. Wagnon, S. Thion, E.J.K. Nilsson, M. Mehl, Z. Serinyel, K. Zhang, P. Dagaut, A.A. Konnov, G. Dayma, W.J. Pitz, Experimental and modeling studies of a biofuel surrogate compound: laminar burning velocities and jet-stirred reactor measurements of anisole, Combust. Flame 189 (2018) 325–336.
[31] M. Nowakowska, O. Herbinet, A. Dufour, P.-A. Glaude, Detailed kinetic study of anisole pyrolysis and oxidation to understand tar formation during biomass combustion and gasification, Combust. Flame 161 (2014) 1474–1488.
[32] Chemkin-Pro 2021R1, ANSYS: Canonsburg, PA, (2021).
[33] I. Wiater, J.G.P. Born, R. Louw, Products, rates, and mechanism of the gas-phase condensation of phenoxy radicals between 500-840 K, Eur. J. Org. Chem. (2000) 921–928.